17th Brazilian Congress of Thermal Sciences and Engineering
November 25th-28th, 2018, Águas de Lindóia, SP, Brazil

ENCIT-2018-0429
AERODYNAMIC ASSESSMENT OF GÖTTINGEN AIRFOIL FOR APPLICATION IN SMALL HORIZONTAL AXIS WINDMILLS

Thiago Canale
Kamal A. R. Ismail
Fatima A. M. Lino
State University of Campinas, Faculty of Mechanical Engineering, Energy Department,
Mendeleiev street, 200, Cidade Universitária "Zeferino Vaz", 13083-860, Barão Geraldo, Campinas - SP, Brazil, Phone: +55 19 3521-3376,
kamal@fem.unicamp.br

Abstract. *The climatic changes, global heating and the associated drastic changes obliged the decision makers to establish policies to reduce ambient aggressions and offensive greenhouse gases (GHG). Intensive research and developments were and still dedicated to reduce GHG emissions and provide sustainable alternative energy sources to the world. Wind energy is at the top of the list since the technology is well developed and accepted by the populations. Much work is still needed to develop efficient and relatively cheap small windmills and popularize their use for generating energy for isolated areas and individual consumers far from the main grid. This paper investigates Göttingen airfoils as alternative airfoils for possible use in small windmills and compares their aerodynamic performance with the SERI airfoils. The blade elements momentum theory was used to evaluate the aerodynamic performance of the windmill rotor. Comparison of the predicted rotors with available data for other rotors indicated that the calculation procedure and the interpolation scheme together with Xfoil are adequate tools for predicting the aerodynamic performance. The results show that the Göttingen airfoil fixation area promotes high mechanical resistance and that the rotor shows narrow tip chord and large root chord and hence light blade tip and strong blade root.*

Keywords: *SERI airfoils family, Göttingen airfoils, small power windmills, isolated areas, wind energy.*

1. INTRODUCTION

Energy is one of the precious inputs for socio-economic development of a country. The rate at which energy is being consumed by a nation often reflects its level of prosperity. The increase of global population is another aspect, which is linked to energy consumption. The rate of change in consumption is slower in developed countries (1.5% per annum) in comparison with developing countries (3.2%) in the last ten years (IEA, 2003; IEA, 2007; UNDP, 2004).

The global energy demand is usually met by a variety of sources. Fossil fuels can meet around 80 per cent of the needs with a small contribution from renewable sources (wind, solar etc.) of about 2.2 %. Fossil fuels are finite and will be completely exhausted in the near future leading to possible global energy crisis.

The power production and energy utilization based on fossil fuels emit to the atmosphere greenhouse gases (GHG) and particulates, responsible for 50 to 60 % of GHG released into the atmosphere on a global basis. With the increase in energy use, atmospheric pollution from the energy sector is expected to increase further in the near future. Several efforts are being realized globally to reduce the level of atmospheric pollution due to human activities by adopting sustainable energy sources like solar and wind among other viable solutions.

Due to the global commitment to reduce GHG emissions and provide sustainable energy sources to the world, efforts are being made to supplement the world energy base with renewable sources. Several countries

have already formulated policies to ensure that renewable sources play an impressive role in the future energy scenario. Wind, is one of the commercially viable and economically competitive renewable sources. The total global installed capacity is 39,434 MW in 2004. Over 73% of the global installations are in Europe. Germany is the European leader, followed by Spain and Denmark.

In recent years, efforts are branched into two main directions: one to build big machines of capacities of few MW, while the second is to use *offshore* technology where wind energy level is stable and high. The first tendency is not as ambient friendly as the second.

In Brazil, the fifth most populated country in the world, has extensive territorial area and low demographic densities in the North and Northeast regions where wind energy potential is high associated with deficient electricity transmission network. In an attempt to preserve the North and Northeast coastal areas from ambient aggressions, Brazil should invest in *offshore* technology. Also, there is a necessity to supply electricity to isolated areas and regions far from the central

grid. This can be achieved by small and medium capacity windmills (1-100kW) where the equipments are relatively simple and the costs of installation and maintenance are acceptable.

The literature review reveals relatively small number of studies related to small power windmills aerodynamics, performance and airfoils in comparison to high capacity windmills. Some old studies of interest to the area of small windmills include Nathan´s (1980) work where he presented a method of determining the blade geometry of a horizontal-axis medium-speed windmill. He used blade element theory and an inversion technique based on defining a local speed ratio at blade elements and in this way he eliminated iterative computation. The theoretical predictions and the experimental results were presented and discussed.

Tangler and Somers (1987) reported the results of numerical study on airfoils intended for application in windmills of 10 to 30 m diameters. Their relative classification was in function of the thickness ratio in the context of the mechanical resistance and wind velocity.

Bruining and Timmer (1992) presented a description of experiments to get quantitative data of the effects of rotation on the lift and drag distribution over the rotor blade. The two-dimensional characteristics of the rotor blade were measured and the same blade was used for the rotating measurements on the rotor test facility. This gave a good comparison of the effects of rotation on the lift and drag distribution. The results were included and discussed.

Somers and Tangler (1995) classified some airfoils as best suited for applications in small power windmills including their position along the rotor blade.

Giguere and Selig (1997) investigated experimentally low Reynolds number airfoils for small horizontal axis windmills. Fuglsang et al. (1998) realized experimental study on airfoils NACA, RISO, FFA and DU for Reynolds number of $1.6x10^6$. In the mean time, Giguere and Selig (1998) realized wind tunnel testing of the airfoils Selig / Giguere SG60xx in the Reynolds number ranging from 10^5 to 5×10^5 and concluded that airfoils SG 6042 and principally SG6043 presented high lift / drag ratios.

Varol et al. (2001) described a study in which the rotational speed of the wind blades can be increased using steering airfoils surrounding the blades. A prototype of this wind turbine was constructed and the steering airfoils were fixed surrounding the blades at an optimum distance. The number of the airfoils and the angle of inclination of the foils were changed. The theoretical and experimental results were discussed.

Selig and Mc Granahan (2004) realized tests on six airfoils to determine their aerodynamic characteristics for use in small windmills. The tests were realized on the following airfoils E387, S822, S834, SD2030, FX63-137, and SH3055.

In order to extract the maximum possible energy from a small windmill, it is important that the blades of the wind turbine start rotating at the lowest possible wind speed. Wright & Wood (2004) realized experimental measurements of the starting performance of a three-bladed, two meter diameter horizontal axis wind turbine and compared the results with calculations using a steady blade element analysis. They concluded that most of the starting torque is generated near the hub, whereas most power-producing torque comes from the tip region.

Kanya and Visser (2010) investigated the impact of airfoil selection on the design of small horizontal axis windmills. Their study was concentrated on NACA4421and SG6043 airfoils. Singh et al. (2012) investigated the effects of the design of a low Reynolds number airfoil for application in small horizontal axis windmills and in their investigation they considered AF300, S1223, S1210, SG6043, and FX63-137 airfoils.

Abdelrahman and Hassanein (2012) investigated the importance of the aerodynamic characteristics of blade airfoil-sections on the design and overall performance predictions of the horizontal-axis wind turbines. They found that the airfoils must exhibit a maximum lift-coefficient and to have a low minimum drag coefficient and/or a high lift/drag ratio. The airfoil section should be designed or selected according to its location along the blade to ensure high contribution to the overall performance of the rotor.

The air viscosity has relatively strong influence on the aerodynamic performance of blades of small wind turbines working under low-Reynolds number conditions. Gu et al. (2012) studied the aerodynamic performance of the airfoil under the low-Reynolds conditions and designed a blade based on the airfoil of the seagull. The CFD results and the analysis showed that the airfoil of the seagull is suitable for the small wind turbine.

Pathike et al. (2013) conducted a study to design a blade suitable for applications in the average wind speed of 3-7 m/s to generate electricity. To design and evaluate performance they used Blade Element Momentum theory and optimized blade shape under constrains that the rotor diameter is not more than 3 m, wind velocity is 6 m/s. They found that, at design wind velocity, the efficiency of the new wind turbine blade was 27% while that of the commercial wind turbine was only 16%.

Pourrajabian et al. (2014) conducted a study to evaluate the influence of variation of the air density on the performance of a small horizontal axis wind turbine blade. Results showed that the performance of a blade optimized for sea level degrades with altitude and that degradation is more important for the starting performance than for the power coefficient.

Bukala et al. (2015) mentioned in their work that in recent years much attention was paid to small wind turbine technology for both individual and private users in Poland. They stressed the need for more awareness campaigns for the users of small turbines.

Small wind turbines are usually installed to produce power irrespective of favorable wind conditions. Karthikeyan et al. (2015) presented a detailed review of various blade profiles and aerofoil geometry optimization processes to achieve high power coefficient in small wind turbines that falls below Reynolds number 500,000.

Hassanzadeh et al. (2016) presented the results of a study to optimize the chord distribution and twist angle of small wind turbine blade to maximize its annual energy production by using a calculation code based on the Blade Element Momentum theory. Results showed the capability of this method to predict the performance of wind turbines.

Shen et al. (2016) optimized the geometry of wind turbine blades in terms of the distribution of the chord and twist angle. A lifting surface method with free wake model was used. Results showed that properly designed blades have a good starting behavior and can increase the annual energy production.

The objective of the present paper is to investigate alternative airfoils for use in small power windmills. The Göttingen airfoils were investigated and compared with the SERI airfoils considered as reference in the present work. The airfoils were treated by using Xfoil then used in a calculation procedure based on Blade Element Momentum Theory (BEM) to estimate the general dimensions, aerodynamic characteristics of windmill rotors and evaluate their energy production and efficiency.

2. CALCULATION PROCEDURE

The calculation procedure is based on pre-determined airfoils characteristics such as C_ℓ, C_d and C_ℓ / C_d. After the airfoils have been defined, an iterative scheme based on the Blade Element Momentum Theory (BEM) and Prandtl's root and tip correction procedure is used. Based on a procedure which follows broadly Wood (2011) and Manwell et al. (2010), a simple numerical home-built code is developed. This code permits calculating the windmill rotor local and overall dimensions, including its aerodynamic characteristics and wind energy annual yield.

Main assumptions and simplifications are listed below

- Radial velocities were neglected;
- The transmission and generator mechanical losses were considered as 10% , a value declared by most manufacturers;
- Incompressible flow;
- The aerodynamic interference of the supporting structure is neglected;
- The first 8% of the blade length are considered for mechanical fixation of the blade and they don't contribute for energy generation;
- Uniform wind velocity over the rotor disc;
- The rotor blades do not deform as a result of the axial force on the rotor; and,
- The rotor blades do not suffer torsion due to the aerodynamic torsion coefficient.

In the calculations, a three bladed rotor was chosen since it offers more stability and smoothness in operation, Fig. 1. The tip velocity ratio was chosen as 6.9 corresponding to wind velocity of 10 m/s as recommended by manufacturers.

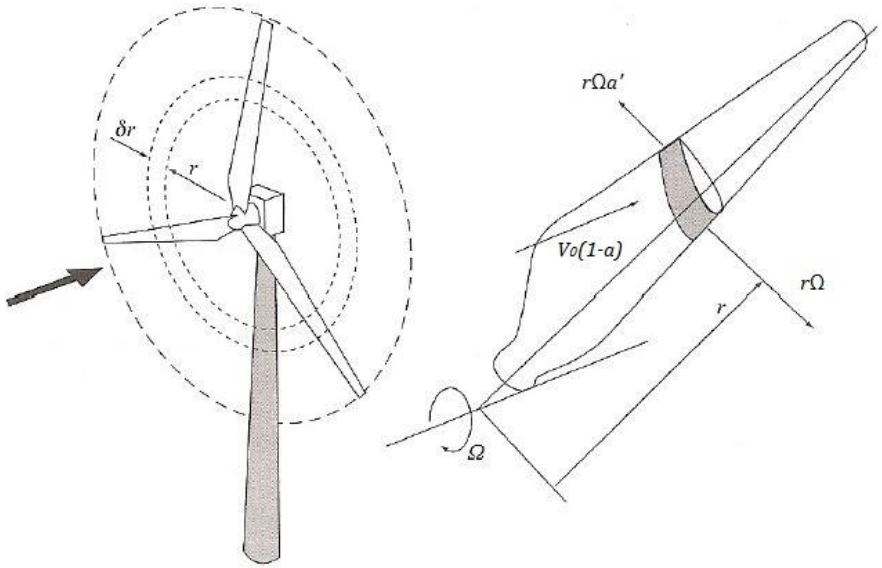

Figure 1. General layout of the windmill rotor.

To start the calculations, the external radius of the windmill is estimated from knowledge of the effective power P and the area swept by the rotor A from Eq. (1)

$$R = \sqrt{\frac{2P}{\rho.\pi.V_0^3.C_P.\eta_m}} \tag{1}$$

Where ρ is the local air density, V_o is the wind speed, C_P is the power coefficient and η_m is the mechanical efficiency (transmission and generator mechanical losses). The power coefficient can be calculated from Eq. 2

$$C_P = \frac{16}{27}.\left[1-\frac{1.386}{B}.sen\left(\frac{\phi}{2}\right)\right]^2.\left[\exp(-0.35.\lambda^{-1,29})-\left(\frac{C_D}{C_L}.\lambda\right)\right] \tag{2}$$

Where B is the number of blades, λ is the tip speed ratio, $\frac{C_D}{C_L}$ is the ratio of the drag coefficient to the lift coefficient and ϕ is the flow angle calculated from Eq. 3

$$\phi = \frac{2}{3}\arctan\left(\frac{1}{\lambda}\right) \tag{3}$$

The values of the interference factors a and a' were assumed zeros to start the numerical calculations while the value of the flow angle ϕ, the local chord and consequently the solidity are calculated

$$\tan(\phi) = \frac{(1-a)}{(1+a').\lambda_r} \tag{4}$$

$$c = \frac{8.\pi.r}{B.C_L}(1-\cos\phi) \tag{5}$$

$$\sigma = \frac{B.c}{2.\pi.r} \tag{6}$$

The airfoil available data is used to estimate the axial and tangential force coefficients C_a and C_t

$$C_a = C_L.\cos\phi + C_D.sen\phi \tag{7}$$

$$C_t = C_L.sen\phi - C_D.\cos\phi \tag{8}$$

The assumed axial interference and tangential interference factors (a) and (a') are then calculated

$$a = \frac{1}{\frac{4.sen^2\phi}{\sigma.C_a}+1} \tag{9}$$

$$a' = \frac{1}{\frac{4.sen\phi.\cos\phi}{\sigma.C_t}-1} \tag{10}$$

The resulting values of (a) and (a') are compared with the assumed values, if the differences are more than the pre-established limit of (10^{-4}) the calculations are repeated until convergence is achieved.

The number of radial elements along the blade length is determined by numerical tests where the number of elements was varied from 20 to 100 in steps of 10. The results were compared for convergence. In the present case, 50 segments were used.

Considering the velocity and forces diagrams shown in Fig. 2, one can calculate the pitch angle (β). From the tip velocity ratio (λ), the wind velocity (V_o) and the rotor external radius (R) one can estimate the rotor rotational speed. Using the converged values of the interference coefficients it is possible to calculate the tangential and axial velocity components U_{tan} and U_{axial} respectively as well as the resultant velocity W .

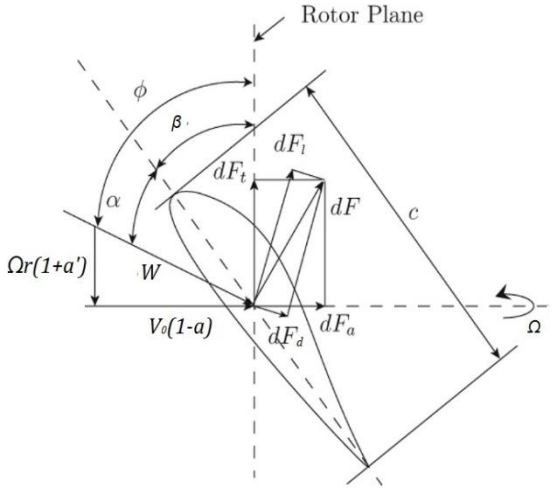

Figure 2. Velocities and forces diagram on airfoil.

Based on the above, the tangential and axial forces on each element dF_t and dF_a are calculated

$$dF_t = 4.\Omega.\rho.V_0.a'(1-a).\pi.r^2.dr \tag{11}$$

$$dF_a = 4.\rho.V_0^2.(a-a^2).\pi.r.dr \tag{12}$$

The losses at the blade tip f_T and at the blade root f_R are estimated by using Prandtl correction factor in terms of the non dimensional element position $\mu=r/R$.

Losses at the tip are given by

$$f_T(\mu) = \frac{2}{\pi}.\cos^{-1}\left(e^{\left(-\frac{B}{2}.\left(\frac{1-\mu}{\mu}\right)\sqrt{1+\frac{(\lambda.\mu)^2}{(1-a)^2}}\right)}\right) \tag{13}$$

while the losses at the blade root are calculated from

$$f_R(\mu) = \frac{2}{\pi}.\cos^{-1}\left(e^{\left(-\frac{B}{2}.\left(\frac{1-\mu_0}{\mu}\right)\sqrt{1+\frac{(\lambda.\mu)^2}{(1-a)^2}}\right)}\right) \tag{14}$$

Where μ_R is the non-dimensional root radius taken as μ_o = *10%* of the blade span according to the preceding assumptions. The element correction factor *f(μ)* is function of the combined losses due to the blade tip ($f_T(\mu)$) and root ($f_R(\mu)$) or

$$f(\mu) = f_T(\mu).f_R(\mu) \tag{15}$$

The net tangential and axial forces are determined by multiplying the respective correction factor by the tangential and axial forces on the blade elements. The contribution of each blade element to the torque *dT* is obtained by multiplying the respective tangential force dF_t *by* its radial position measured from the center of rotation of the rotor *r*. The power

generated by the rotor (P) is the product of the total torque (T) (which is the sum of the elements individual contributions) times the rotor rotational speed *Ω*. Hence one can calculate the power and torque coefficients C_P *and* C_q as below

$$dT = dF_t.r \tag{16}$$

and the total torque is given by

$$T = \sum_{r=r_o}^{R} dT$$

The power generated by the rotor is the product of the total torque (T) times the rotor rotational speed *Ω or*

$$P = T.\Omega \tag{17}$$

The power and torque coefficients C_P *and* C_q *can be calculated from*

$$C_P = \frac{2.P}{V_0^3.\pi.R^2} \tag{18}$$

$$C_q = \frac{C_p}{\Omega} \tag{19}$$

This calculation procedure is implemented in a simple home-built code to calculate the windmill rotor local and overall dimensions as well as its aerodynamic characteristics.

3. VALIDATION OF THE MODEL AND METHOD OF CALCULATION

In order to validate the numerical home built code the numerical predictions were compared with the experimental results from Hand et al. (2001) and Anderson et al. (1981). The rotor analyzed by Hand et al. (2001) has S 809 airfoil section and rotor diameter of 10 m operating at 72 rpm and wind velocities in the range of 6 to 25 m/s. The rotor in the Anderson et al. (1981) study has a rotor with NACA 4412 airfoil and operating at tip speed ratio varying between 6 to 14.

The present numerical predictions were also compared with the numerical results from Lindenburg (2003) for the rotor with S 809 airfoil and with the results from Wood (2011) for rotor with NACA 4412 airfoil. The distributions of chord and pitch angle used by Lindenburg (2003) as shown in Fig. 3, are the same used in the present method for the calculations of the S809 and GO447 used in the comparisons.

The airfoil S 809 is considered as a reference airfoil since it has both experimental and numerical data. The torque generated by the utilizing this airfoil was also calculated by the present method. As can be seen the agreement with the experiments is good. The investigated Gottingen airfoil shows higher values of power than the reference airfoil case. This is due to the fact that with the increase of the velocity the frictional losses increase with lower rates than in the reference airfoil resulting in significant increase in torque.

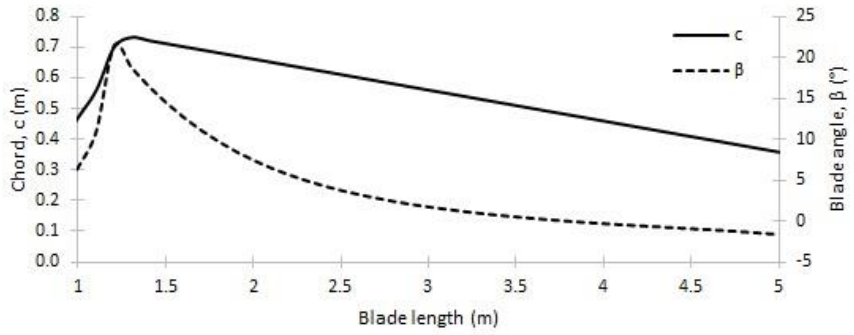

Figure 3. The distributions of chord and pitch angle along the blade used for the comparison with Lindenburg (2003), Hand et al. (2001) and present work.

Figure 4 show comparative results of the predicted power coefficient with experimental and numerical results of the reference airfoil S809. As can be seen the predicted results by the present method agrees with the experimental results and also with Lindenburg´s work (2003) numerical predictions. As can be verified the average difference between the present predictions and the experimental results is about 0.1% while the average difference between Lindenburg´s results and the experiments is about 0.6%. One can also observe that the values of the power coefficients for the investigated airfoils are higher than those of the reference airfoil for the same reasons mentioned before.

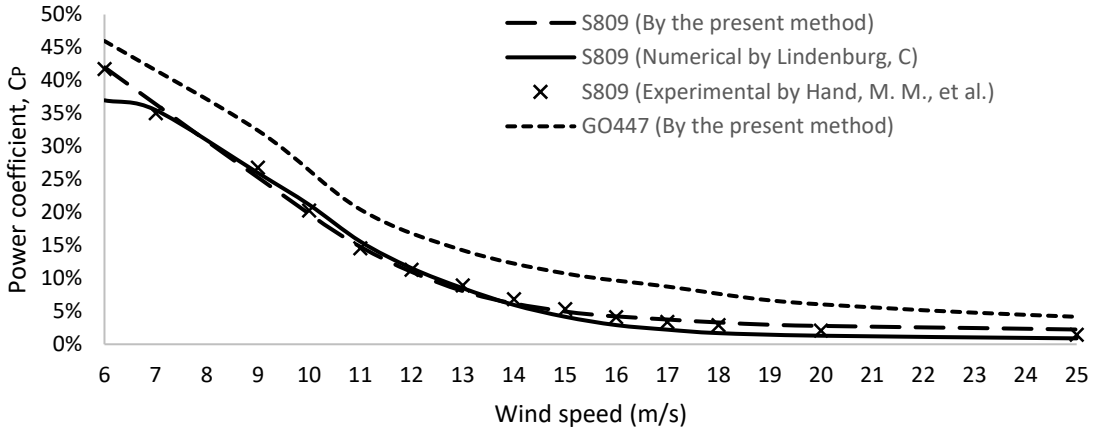

Figure 4. Comparison of the predicted power coefficient with available experimental and numerical results.

Anderson (1981) carried out experimental tests on a Double blade rotor with NACA 4412 airfoil at a Constant velocity of 10 m/s while the tip speed ratio was varied in the range 6-14. The variation of the chord c and the pitch angle β of the rotor are shown in Fig. 5.

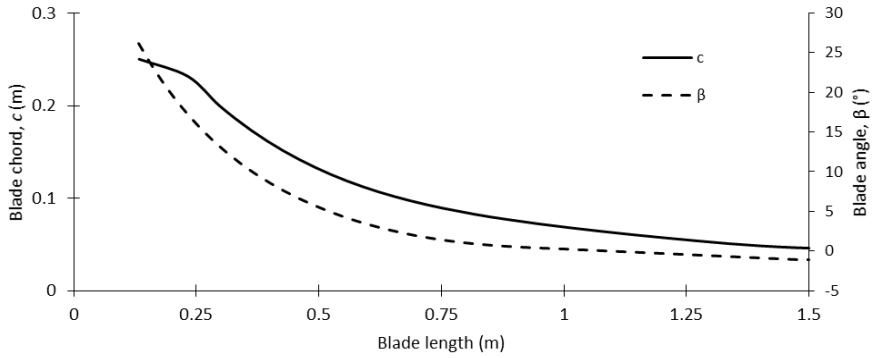

Figure 5. The distributions of chord and pitch angle along the blade used for the comparison with Wood (2011), Anderson et al. (1981) and the present work.

In order to validate the present method of calculation and the performance of the airfoil GO447, the chord and pitch angle distributions were used to calculate the power and the coefficient of power of these airfoils and compare with the results of the NACA 4412 based rotor as shown in Figs. 6 and 7. As can be seen in Fig. 6 the NACA rotor calculated by the present method agrees well with the experimental results for the tip speed range 7 to 11. At higher tip speed ratios the differences are bigger due to the precision of the corrections at the tip region, while the numerical predictions by Wood (2011) seem to agree well over a wider range of tip speed ratio extending from 6 to 13.

The rotors based on the airfoil GO447 show higher power and power coefficient for tip speed range below $\lambda = 10$. The use of the chord and pitch angle distributions β as used in the calculation of the rotor based on the NACA 4412 resulted in higher solidity of the investigated airfoil enhancing the power and power coefficient at tip speed ratios below about a value of 10. For higher tip speed ratios, that is more than 10 the friction losses increase due to the solidity ratio and this reduces the generated power and the power coefficient as can be verified in Figs. 8 and 9.

The present predictions agree well with available experimental and numerical results and this validates the numerical code and the numerical predictions.

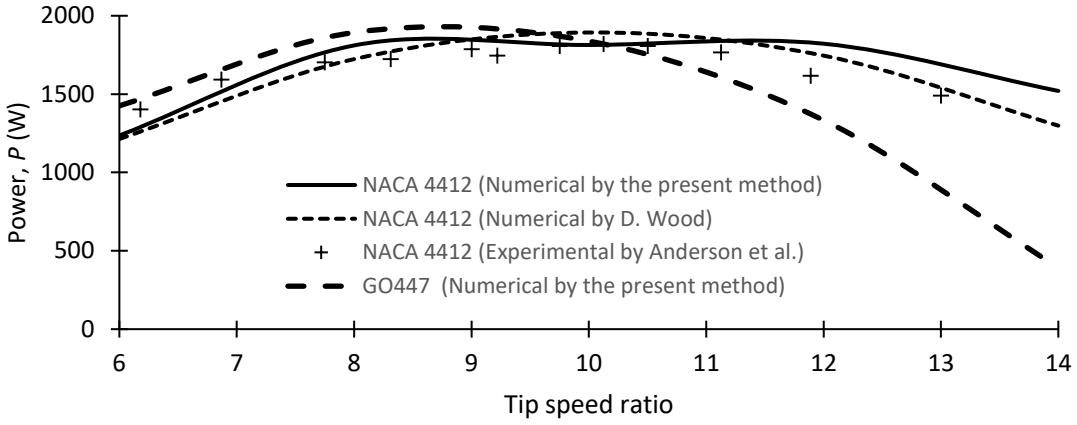

Figure 6. Comparison of the predicted power with available experimental and numerical results.

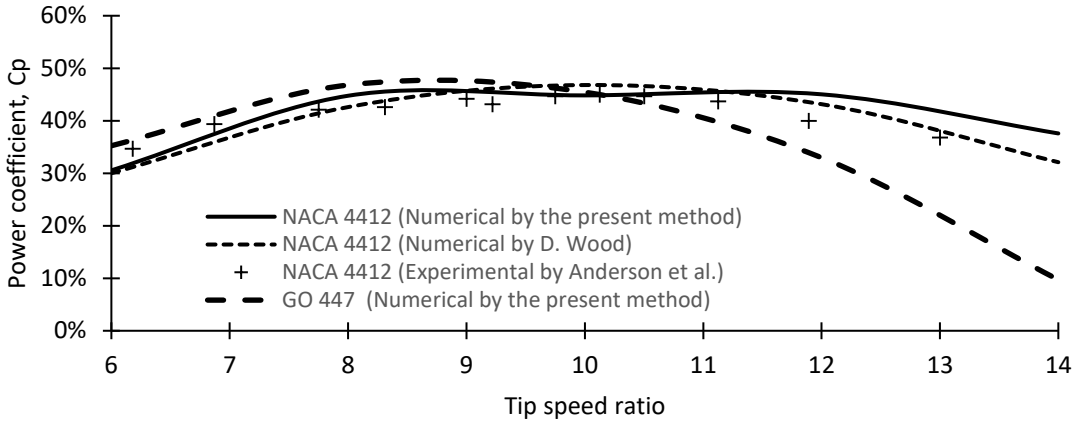

Figure 7. Comparison of the predicted power coefficient with available experimental and numerical results.

4. CHOICE AND ANALYSIS OF AIRFOILS

In the present study a three blade rotor of a small horizontal axis windmill is calculated based on the investigated airfoils. The rotor blade is composed of three regions: root, central and tip regions for each of which one specific airfoil section is used. For the SERI rotor (based on reference airfoil), the blade root region covers the first 20% of the blade length and uses the thick airfoil S 807 for mechanical construction reasons. The second region (central) covers the distance from 20% to 95% of the blade length and uses the S 805A airfoil. The third region (tip region) covers 95-100% of the blade length and uses the S 806A airfoil. In the case of the Göttingen rotor, the blade is composed of GO 255 at the root, GO 447 airfoil at the central region and GO 500 airfoil at the tip region. The relevant aerodynamic data of the SERI and Göttingen airfoils were generated by Xfoil for Reynolds number 1 x 10^6. For intermediate stations within each of the three regions, the relevant aerodynamic data is obtained by interpolation using the Xfoil program.

5. RESULTS AND DISCUSSION

Table 1 presents the data used in the calculation procedure.

Table 1. General data of the investigated rotors

Parameter	Symbol	Value
Nominal power (kW)	P	50
Wind speed (m/s)	V_o	10
Air temperature for altitude range of 50-300 m (K)	T_{air}	297
Mechanical efficiency	η_m	90%
Number of blades	B	3
Tip speed ratio	λ	6,9
Root radius of the blade (m)	r_1	0,64
Adopted rotor radius (m)	R	8

5.1. ANALYSIS OF AIRFOILS SECTIONS

As mentioned before, the blades are composed of three regions; root, central and tip and for each region one airfoil is used according to the local requirement. Thus, each blade of each rotor is composed of three airfoils of the same family.

5.1.1. BLADE ROOT AIRFOILS

Figs. 8 and 9 show the two airfoils S807 and GO255 used for the root region have respectively, 18 and 19% maximum thickness ratio. The airfoil S 807 has both smaller thickness and smaller ratio of projected profile area to chord; hence, the mechanical resistance is lower than that of the GO255 airfoil.

The airfoil cambers are notably different for the two airfoils, with the Göttingen family airfoils GO255 having camber of 4.7% and showing curvature up to 60% of the chord length. The airfoil S807 has camber of 1.9% and constant curvature up to 30% of the chord length followed by straight surface up to the trailing edge. These geometrical characteristics make this airfoil easy to manufacture in comparison with the Göttingen airfoil.

The pressure distribution and the aerodynamic characteristics such as lift, drag coefficients and the ratio of lift/drag are affected by the camber and the thickness distribution along the chord. The airfoil S807 shown in Fig. 8 has a nearly flat top surface. For angle of attack of 9.6° it indicates coefficients of lift and drag of 1.3996 and 0.01309, respectively, while the lift to drag ratio is about 106.95.

From Fig. 9 for the airfoil GO255 at an angle of attack of 5.25° it shows a lift and drag coefficients of 1.0881 and 0.00893, respectively. The lift to drag ratio is about 121.87, about 14.1% higher than that of the S807airfoil.

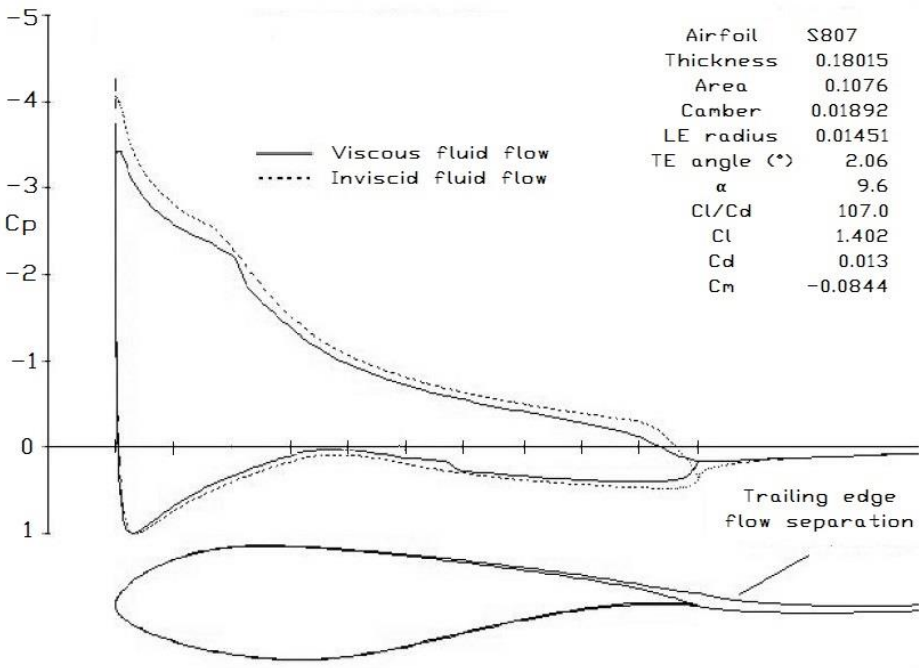

Figure 8. Pressure distribution on the S807 airfoil in the root region for viscous and inviscid flow conditions .

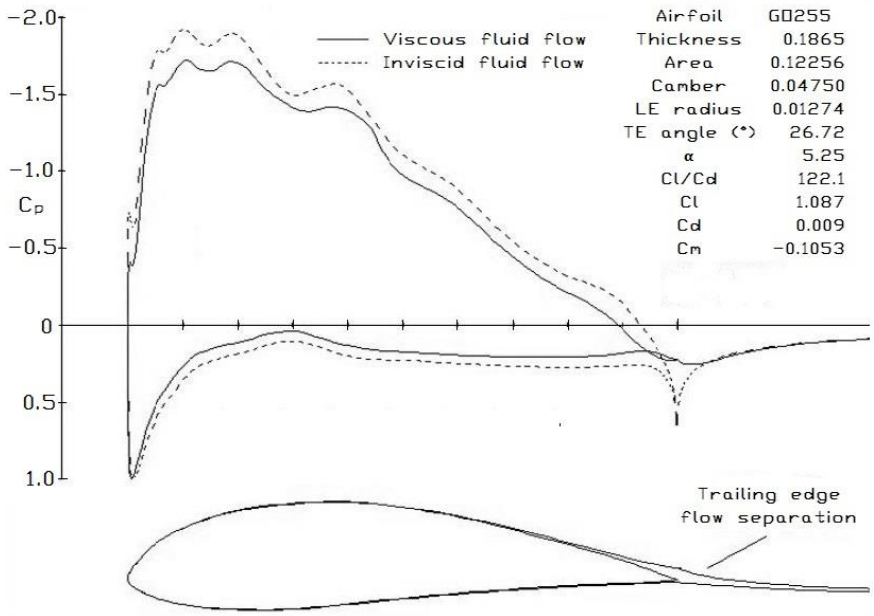

Figure 9. Pressure distribution on the GO255 airfoil in the root region for viscous and inviscid flow conditions.

5.1.2. AIRFOILS FOR THE CENTRAL REGION OF THE BLADE

The airfoils S805A and GO447 adopted for the central region of the blade have maximum thickness ratios of 13.5% and 12.7% respectively. Figs. 10 and 11 shows that the airfoil S805A has a camber of 2.1%, or 9.5% smaller than that of the airfoil GO447. High camber ratio will produce high lift coefficient and high drag coefficient too.

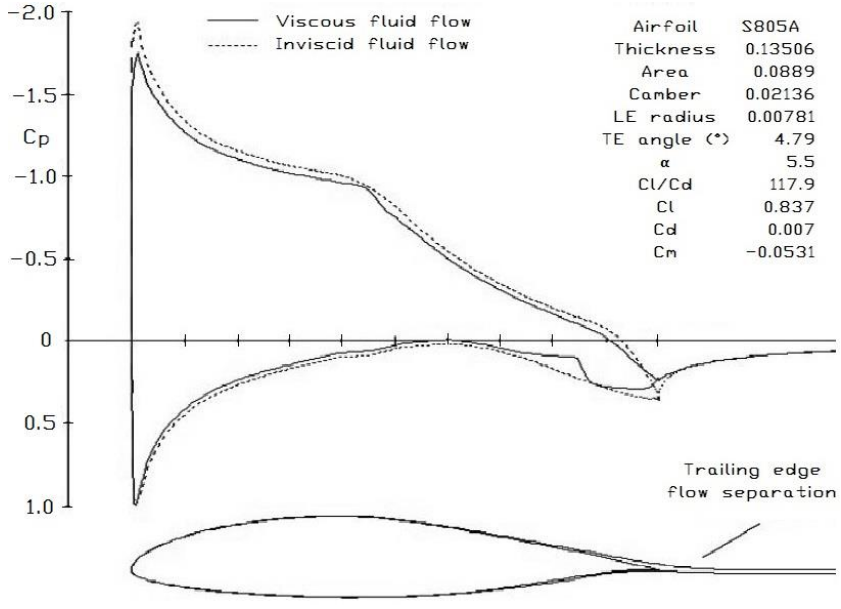

Figure 10. Pressure distribution on the S805A airfoil for the blade central region.

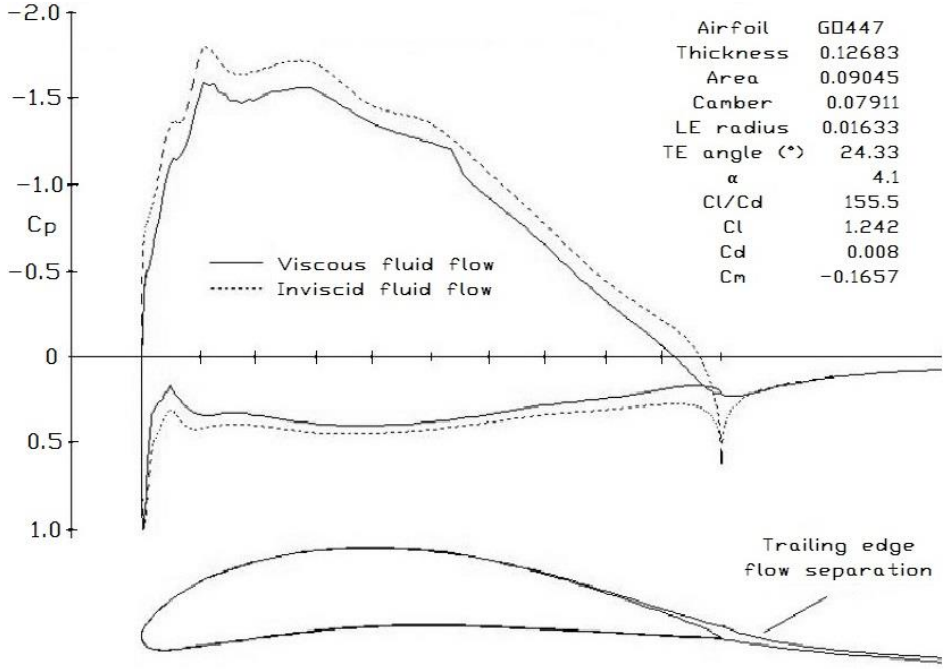

Figure 11. Pressure distribution on the GO447 airfoil for the blade central region.

The airfoil S805A has a ratio of lift to drag coefficients of 117.13, coefficients of drag and lift of 0.00743 and 0.8698, respectively, at angle of attack of 5.5º. These values are smaller than those of the GO447 airfoil.

The GO 447 airfoil, Fig. 11 has lift and drag coefficients more than that of S807. The value of the ratio of lift to drag coefficients is about 153.78 or 23.9% higher than those of S807 occurring at angle of attack of 4.1°. The corresponding drag and lift coefficients for this angle are 0.00805 and 1.2381, respectively.

5.1.3. BLADE TIP AIRFOILS

The airfoils investigated for the blade tip shown in Figs. 12 and 13, are S806A and GO500. The small camber of S806A reduces the turbulent effects near the trailing edge. The airfoil S806A has a maximum thickness ratio of 11% while the GO500 has a maximum thickness ratio of 10%. As a result S806A airfoil is heavier than the GO500 airfoil. The airfoil S806A shows little camber and produces less lift at the tip and consequently sheds less tip vortices in comparison with GO500 airfoil.

The pressure distribution of the S806A airfoil is only relatively high at the leading edge region and decreases gradually down to the trailing edge. This distribution of pressure, shown in Fig. 12, reduces the maximum value of C_ℓ / C_d to a value of 107.2 occurring at angle of attack of 3.2º while the corresponding lift and drag coefficients are 0.5708 and 0.00527, respectively.

The pressure distribution for airfoil GO500 is shown in Fig. 13. The angle of attack for maximum ratio of lift to drag occurs at 2.6º for which the drag and lift coefficients are 0.00574 and 1.0116, respectively, while the maximum ratio of the lift to drag coefficients is 176.1 nearly 62.9% more than that of airfoil S806A. This permits using a smaller chord and hence less weight at the tip.

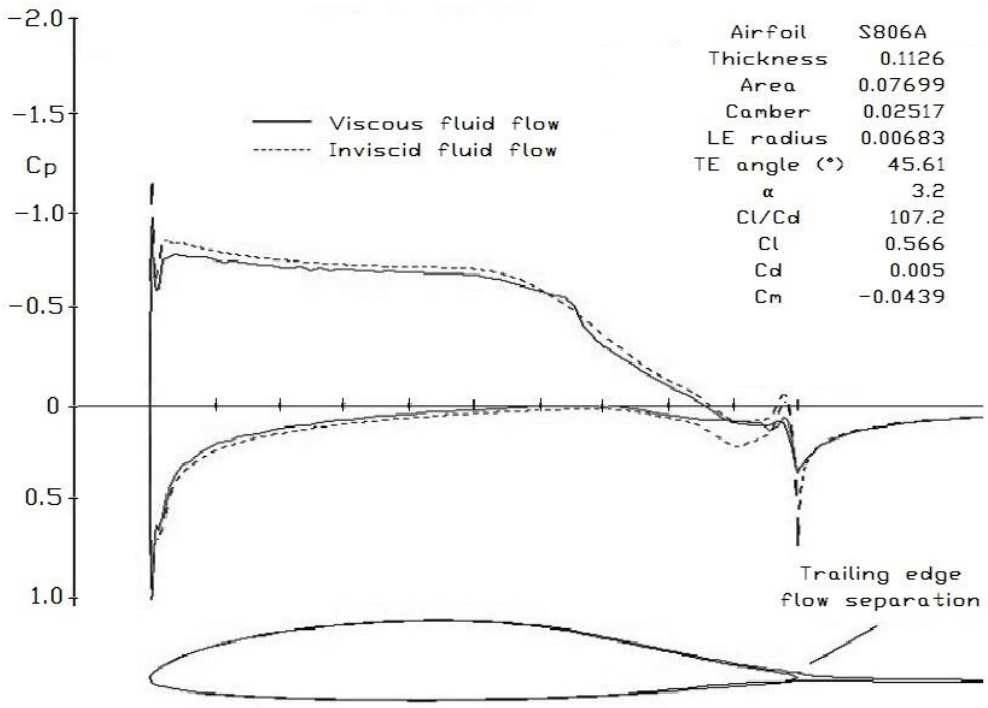

Figure 12. Pressure distribution on the S806A airfoil for the blade tip region.

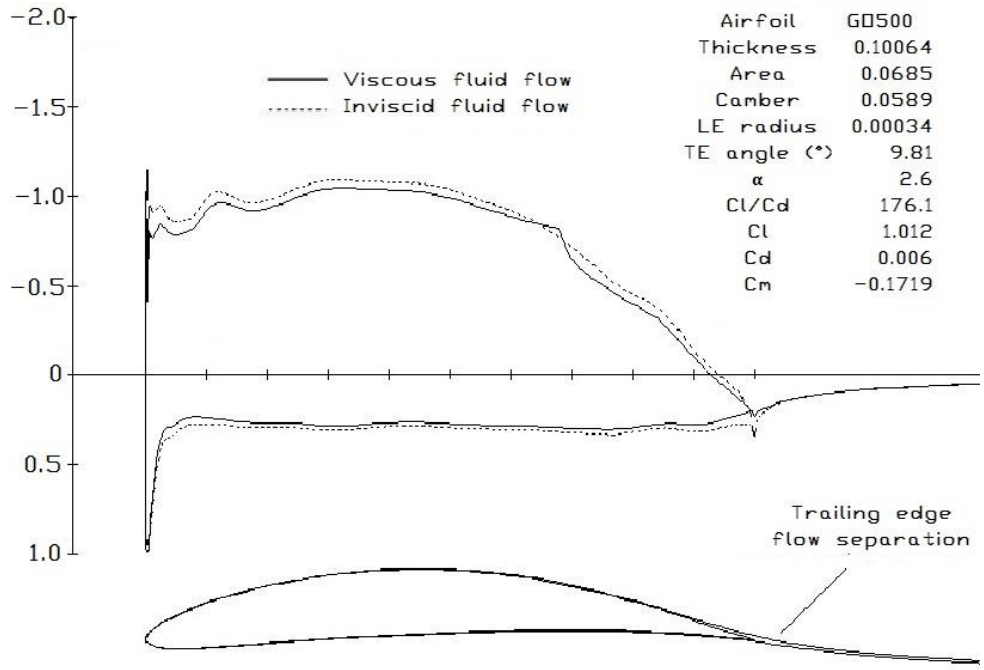

Figure 13. Pressure distribution on the GO 500 airfoil for the blade tip region.

Summary of the main aerodynamic characteristics of the investigated airfoils is presented in Table 2.

Table 2. Aerodynamic characteristics of investigated airfoils

Geometric properties							
Rotor	Blade length	Airfoil	Chord (m)	Thickness (m)	Area (m^2)	Camber (m)	Leading edge radius (m)
	20% Root (0.8m)	GO255	1.239	0.2311	0.1519	0.0589	0.0158

Göttingen	20-95% Central (5.92m)	GO447	0.331	0.0420	0.0299	0.0262	0.0054
	95 - 100% Tip (8m)	GO500	0.330	0.0332	0.0226	0.0194	0.0001
SERI	20% Root (0.8m)	S807	0.961	0.1731	0.1034	0.0182	0.0139
	20-95% Central (5.92m)	S805A	0.473	0.0639	0.0420	0.0101	0.0037
	95 - 100% Tip (8m)	S806A	0.545	0.0614	0.0420	0.0137	0.0037

Relative to chord geometric properties							
Rotor	Blade length	Airfoil	Thickness	Area	Camber	Leading edge radius	Trailing edge angle (°)
Göttingen	20% Root (0.8m)	GO255	0.1865	0.12256	0.04750	0.01274	26.72
	20-95% Central (5.92m)	GO447	0.12683	0.09045	0.07911	0.01633	24.33
	95-100% Tip (8m)	GO500	0.10064	0.0685	0.0589	0.00034	9.81
SERI	10% Root (0.8m)	S807	0.18015	0.1076	0.01892	0.01451	2.06
	20-75% Central (5.92m)	S805A	0.13506	0.0889	0.02136	0.00781	4.79
	95-100% Tip (8m)	S806A	0.11259	0.07699	0.02517	0.00683	45.61

Max. lift to drag aerodynamics properties							
Rotor	Blade length	Airfoil	A (°)	Cl/Cd	Cl	Cd	Cm
Göttingen	20% Root (0.8m)	GO255	5.25	122.1	1.087	0.009	-0.1053
	20-95% Central (5.92m)	GO447	4.1	155.5	1.242	0.008	-0.1657
	95-100% Tip (8m)	GO500	2.6	176.1	1.012	0.006	-0.1719
SERI	20% Root (0.8m)	S807	9.6	107.0	1.402	0.013	-0.0844
	20-75% Central (5.92m)	S805A	5.5	117.9	0.837	0.007	-0.0531
	95-100% Tip (8m)	S806A	3.2	107.2	0.566	0.005	-0.0439

5.2. ROTOR ANALYSIS BASED ON THE INVESTIGATED AIRFOILS

The two airfoils families investigated are used to design three bladed windmill rotors to generate 50kW with wind velocity of 10 m/s, blade length of 8m and tip velocity ratio of 6.9, determined from a previous evaluations.

By using Eq. 4, Fig. 14 was generated for the distribution of flow angle along the blade length for the two airfoils. As can be seen, there is practically no variation due to profile change. The angle at the root is about 36.96° and flow angle at the tip is about 5.50°.

Figure 14. Variation of the relative flow angle along the blade length for the two airfoils.

Figure 15 shows the variation of blade angle along the blade length for the two airfoils. The Göttingen airfoil shows a relatively bigger blade angle than the SERI airfoil. Smaller blade angle helps keeping the flow in contact with the blade surface at the leading edge and hence better aerodynamic performance of the blade. The abrupt discontinuities are due to the interpolation scheme of the airfoil data.

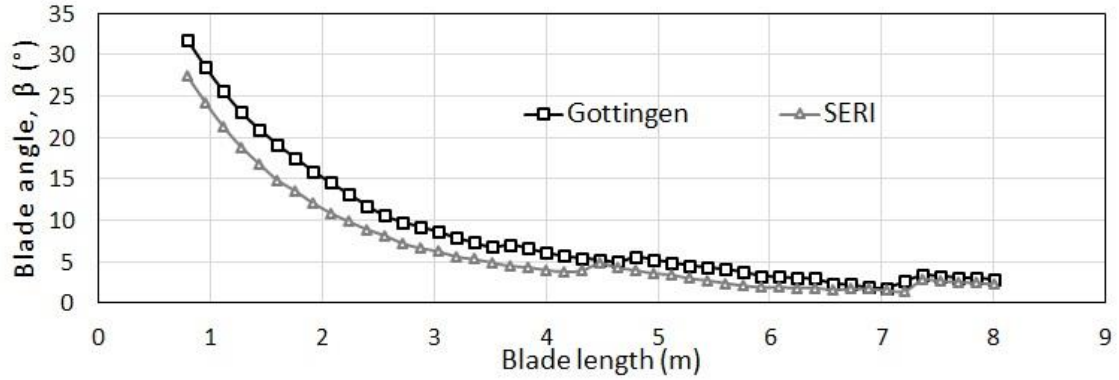

Figure 15. Distribution of the blade angle along the blade length for the two airfoils.

Calculation of the resultant velocity for the two profiles shows little variation along the blade length as can be seen in Fig.16. The tip velocity is found to be 69 m/s or a Mach number of 0.2072, which is below the compressibility limit.

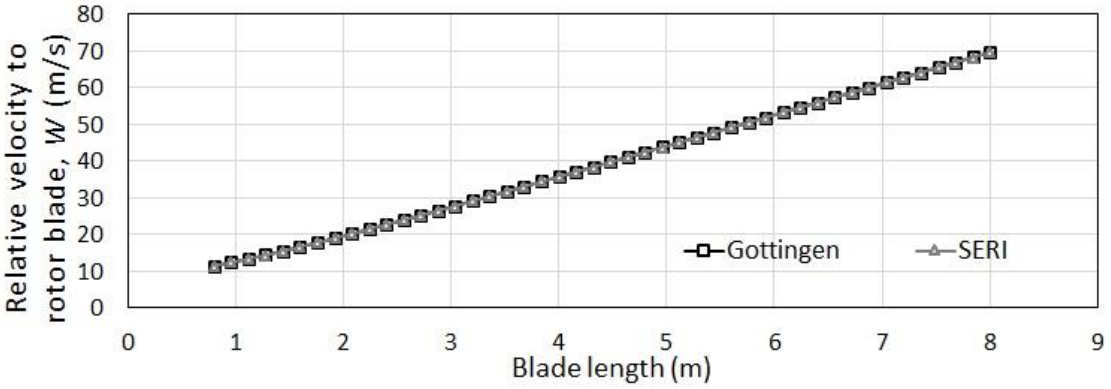

Figure 16. Variation of the relative velocity along the blade length for the two airfoils.

The local aerodynamic chord of each of the investigated airfoils is calculated along the blade length as in Fig. 17. One can observe that the root chord of the Göttingen airfoil is 1.24 m and its chord at tip is 0.3 m. In the case of SERI profile the tip chord is 0.54 m much bigger than that of the Göttingen airfoil and consequently results in a heavier rotor. Also, the root region of the Göttingen airfoil has bigger chord which is beneficial for blade fixation. The local abrupt variations along the curves in Fig. 17 are due to numerical interpolation of airfoil data.

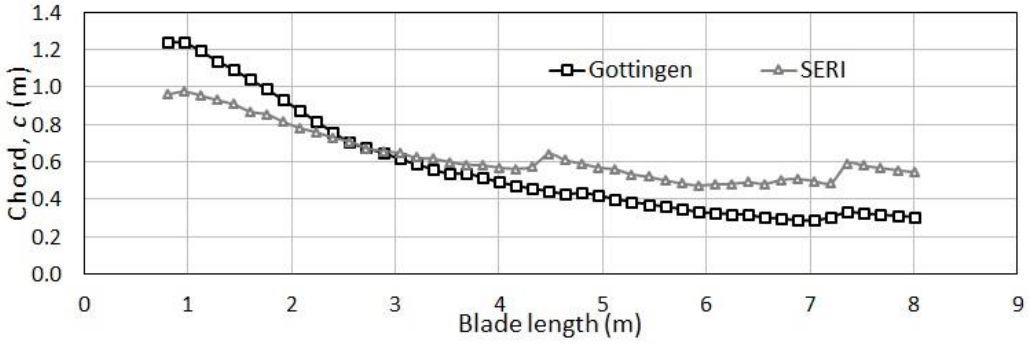

Figure 17. Chord distribution along the blade length for the two airfoils.

The distribution of the axial aerodynamic coefficient along the blade chord for the two airfoils is shown in Fig. 18. The Göttingen airfoil also shows a constant axial loading coefficient of 1.2 in the middle part of the blade due to moderate camber in this region, falling to values of 0.85 and 1.01 at the root and tip, respectively. This distribution leads to high bending moment on the blades. Again, the abrupt changes are due to data interpolation scheme.

The SERI blade shows a continuously decreasing axial coefficient along the blade from 1.1 at the blade root to 0.55 at the tip. This axial force coefficient provokes less bending moment on the rotor base and the supporting structure.

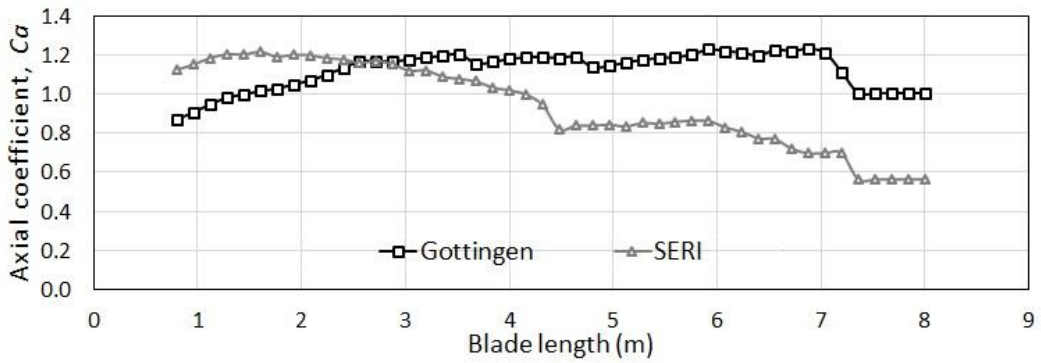

Figure 18. Variation of the axial aerodynamic coefficient along the blade length for the two airfoils.

The tangential aerodynamic coefficients of the two rotors are decreasing along the blade length showing tangential loading at the tip nearly of the same order as shown in Fig. 19.

The SERI and Göttingen airfoils show nearly the same axial and tangential interference factors and the graphs are omitted for brevity.

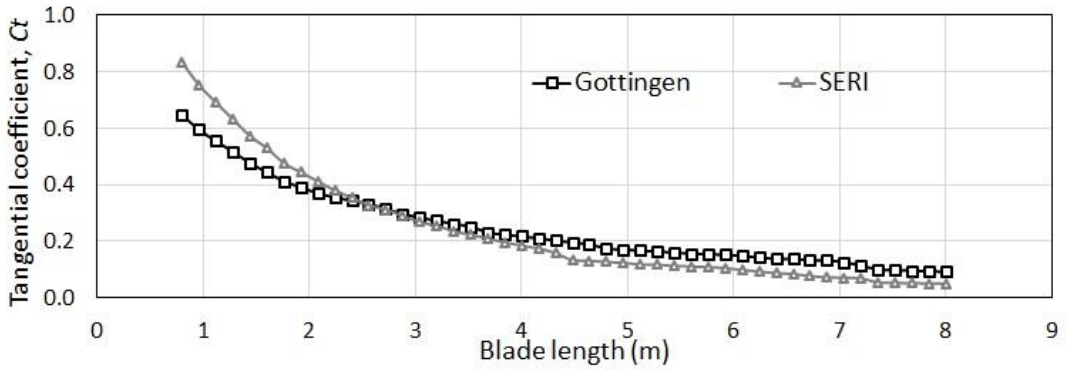

Figure 19. Variation of the tangential aerodynamic coefficient along the blade length for the two airfoils.

Since the axial interference factors for the two rotors are very close, the resulting axial loadings are also close one to the other. The axial loading is 9189N for the Göttingen rotor and 9190N for the SERI rotor. The two distributions show a maximum value of axial loading of 327N at a radial position of 6.88m from the rotor axis as can be seen in Fig. 20.

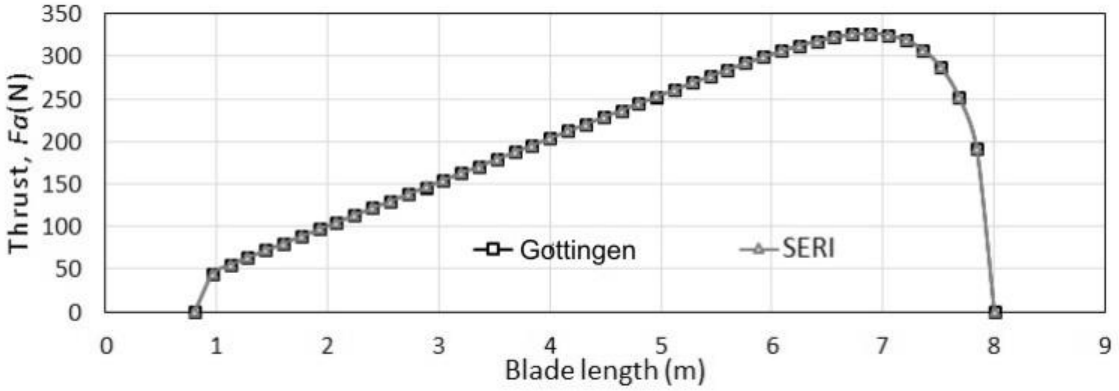

Figure 20. Thrust variation along the blade length for the two airfoils.

Figure 21 shows that the rotor based on SERI airfoil has low tangential force all along the blade and in average 1.52% lower than Göttingen airfoil. The total tangential force over the SERI and Göttingen rotors are respectively 1521.55N and 1545.07N.

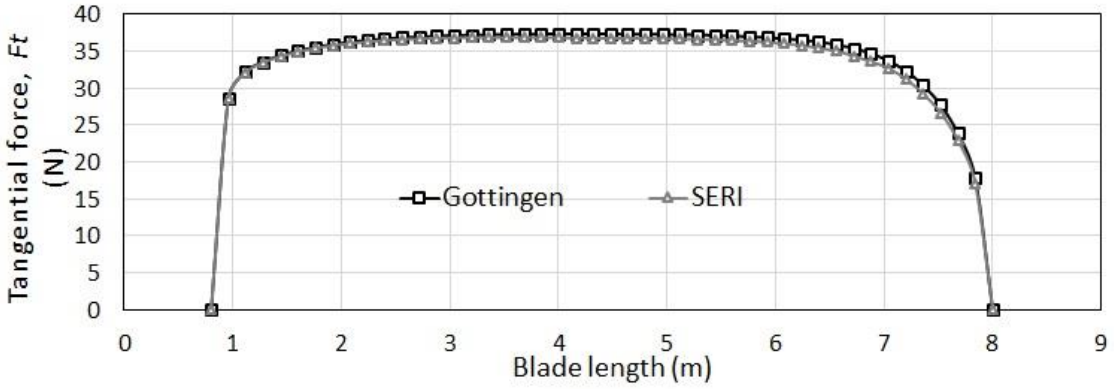

Figure 21. Tangential force distribution along the blade length for the two airfoils.

Figure 22 shows the torque distribution along the blade. The total integrated torque of the Göttingen rotor is 6681.32 N.m, while the torque developed by the SERI rotor is 6551.64 N.m, about 1.9% less than that of the Göttingen rotor.

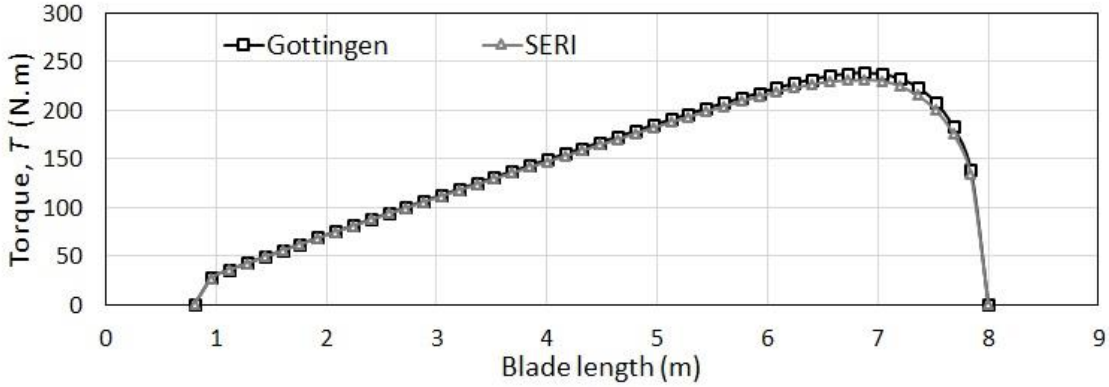

Figure 22. Torque distribution along the blade length for the two airfoils.

The power generated by the two rotors, Fig. 23, can be estimated from the torque and the rotational speed. The Göttingen rotor can generate 57.62 kW, while the SERI rotor generates 56.50 kW. Their respective power coefficients are 50.08%, and 49.11%. Assuming a wind velocity of 10 m/s (considered constant for only assessment) and that the windmill is rotating at its operational speed 80% of the time, one can estimate the annual electricity generated. The SERI rotor can generate 356.4 MWh, while the Göttingen rotor can generate 363.4 MWh.

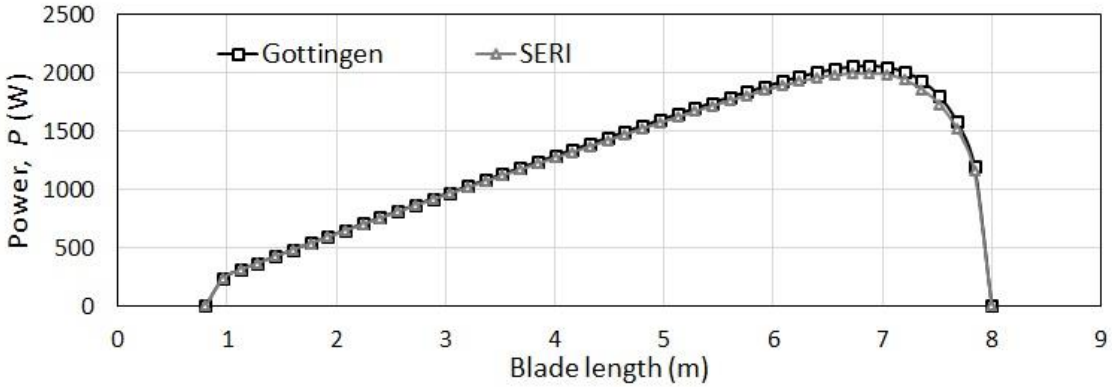

Figure 23. Power distribution along the blade length for the two airfoils.

6. CONCLUSIONS

Comparison of the predicted rotors based on the investigated airfoils with available results from other rotors indicates that the calculation procedure and the interpolation scheme together with Xfoil are adequate tools for predicting the aerodynamic performance and preliminary design of small windmills.

The geometry of the Göttingen rotor show narrow tip chord which results in a light blade tip in comparison with SERI rotor.

The fixation area per unit chord for Göttingen GO255 root airfoils is bigger than that of SERI S807 root airfoil, which results in higher mechanical resistance at the blade root.

7. ACKNOWLEDGEMENTS

The authors wish to thank the CNPq for the PQ Research Grant to the second author and the Pos doc Grant to the third author.

8. REFERENCES

Abdelrahman, M., & Hassanein, A., 2012. Aerodynamics of airfoil sections and their influence on wind turbine design and performance. International Journal of Engineering Systems Modelling and Simulation, 4(3), 113-119.

Anderson, M. B., 1981. Experimental and theoretical study of horizontal-axis wind turbines (Doctoral dissertation, University of Cambridge).

Bruining, A., & Timmer, W. A., 1992. Airfoil characteristics of rotating wind turbine blades. Journal of Wind Engineering and Industrial Aerodynamics, 39(1-3), 35-39.

Bukala, J., Damaziak, K., Kroszczynski, K., Krzeszowiec, M., & Malachowski, J., 2015. Investigation of parameters influencing the efficiency of small wind turbines. Journal of Wind Engineering and Industrial Aerodynamics, 146, 29-38.

Fuglsang, P., Antoniou, I., Dahl, K. S., & Madsen, H. A., 1998. Wind Tunnel Tests of the FFA-W3-241, FFA-W3-301 and NACA 63-430 Airfoils. RISO-REPORTS-RISO R.

Giguere, P., & Selig, M. S., 1997. Low Reynolds number airfoils for small horizontal axis wind turbines. Wind Engineering, 367-380.

Giguere, P., & Selig, M. S., 1998. New airfoils for small horizontal axis wind turbines. Journal of solar energy engineering, 120(2), 108-114.

Gu, R., Xu, J. L., & Yang, Y. B., 2012. The investigation of the small bionic wind turbine based on the seagull airfoil. In Advanced Materials Research (Vol. 347, pp. 3533-3539). Trans Tech Publications.

Hand, M. M., Simms, D. A., Fingersh, L. J., Jager, D. W., Cotrell, J. R., Schreck, S., & Larwood, S. M., 2001. Unsteady aerodynamics experiment phase VI: wind tunnel test configurations and available data campaigns (No. NREL/TP-500-29955). National Renewable Energy Lab., Golden, CO.(US).

Hassanzadeh, A., Hassanabad, A. H., & Dadvand, A., 2016. Aerodynamic shape optimization and analysis of small wind turbine blades employing the Viterna approach for post-stall region. Alexandria Engineering Journal, 55(3), 2035-2043.

IEA, 2003. Energy balances of non-OECD Countries 2000-2001, International Energy Agency, Paris.

IEA, 2007. Key world energy statistics, International Energy Agency, Paris.

Kanya, B., & Visser, K., 2010. The Impact of Airfoil Selection on the Design of Small Horizontal Axis Wind Turbines. In 48th AIAA Aerospace Sciences Meeting Including the New Horizons Forum and Aerospace Exposition (p. 1583).

Karthikeyan, N., Murugavel, K. K., Kumar, S. A., & Rajakumar, S., 2015. Review of aerodynamic developments on small horizontal axis wind turbine blade. Renewable and Sustainable Energy Reviews, 42, 801-822.

Lindenburg, C., 2003. Investigation into rotor blade aerodynamics. ECN Report: ECN-C-03-025.

Manwell, J. F., McGowan, J. G., & Rogers, A. L. (2010). Wind energy explained: theory, design and application. John Wiley & Sons.

Nathan, G. K., 1980. A simplified design method and wind-tunnel study of horizontal-axis windmills. Journal of Wind Engineering and Industrial Aerodynamics, 6(3-4), 189-205.

Pathike, P., Katpradit, T., Terdtoon, P., & Sakulchangsatjatai, P., 2013. A new design of blade for small horizontal-axis wind turbine with low wind speed operation. Energy Research Journal, 4, 1-7.

Pourrajabian, A., Mirzaei, M., Ebrahimi, R., & Wood, D., 2014. Effect of air density on the performance of a small wind turbine blade: A case study in Iran. Journal of Wind Engineering and Industrial Aerodynamics, 126, 1-10.

Selig, M. S., & McGranahan, B. D., 2004. Wind tunnel aerodynamic tests of six airfoils for use on small wind turbines. Journal of solar energy engineering, 126(4), 986-1001.

Shen, X., Yang, H., Chen, J., Zhu, X., & Du, Z., 2016. Aerodynamic shape optimization of non-straight small wind turbine blades. Energy Conversion and Management, 119, 266-278.

Singh, R. K., Ahmed, M. R., Zullah, M. A., & Lee, Y. H., 2012. Design of a low Reynolds number airfoil for small horizontal axis wind turbines. Renewable energy, 42, 66-76.

Tangler, J. L., & Somers, D. M., 1987. Status of the special-purpose airfoil families (No. SERI/TP-217-3264; CONF-871062-9). Solar Energy Research Inst., Golden, CO (USA); Airfoils, Inc., Hampton, VA (USA).

Tangler, J. L., & Somers, D. M., 1995. NREL airfoil families for HAWTs (No. NREL/TP--442-7109). National Renewable Energy Lab., Golden, CO (United States).

UNDP, 2004. World energy assessment: overview, World Energy Council update. Bureau for development policy, New York, pp. 25-31.

Varol, A., İlkılıç, C., & Varol, Y., 2001. Increasing the efficiency of wind turbines. Journal of Wind Engineering and Industrial Aerodynamics, 89(9), 809-815.

Wood, D., 2011. Small wind turbines, Analysis, design and application, Springer-Verlag London, Limited.

Wright, A. K., & Wood, D. H., 2004. The starting and low wind speed behaviour of a small horizontal axis wind turbine. Journal of Wind Engineering and Industrial Aerodynamics, 92(14-15), 1265-1279.

9. RESPONSIBILITY NOTICE

The authors are the only responsible for the printed material included in this paper.